Quantitative trait loci mapping and candidate gene analysis of stoma-related traits in wheat (*Triticum aestivum* L.) glumes

Ning Li [1], **Fanfan Dong** [1], **Tongtong Liu** [2], **Jinwen Yang** [1], **Yugang Shi** [1], **Shuguang Wang** [1], **Daizhen Sun** [Corresp., 1], **Ruilian Jing** [3]

[1] College of Agronomy, Shanxi Agricultural University, Taigu, China

[2] College of Food Science and Engineering, Shanxi Agricultural University, Taigu, China

[3] National Key Facility for Crop Gene Resources and Genetic Improvement/Institute of Crop Sciences, Chinese Academy of Agricultural Sciences, Beijing, China

Corresponding Author: Daizhen Sun
Email address: sdz64@126.com

The photosynthesis of wheat glumes makes important contributions to the yield. Stomata play a crucial role in regulating photosynthesis and transpiration in plants. However, the genetic base of wheat glume stomata is not fully understood. In this study, stomatal length (SL), stomatal width (SW), stomatal density (SD), potential conductance index (PCI) of stomata, stomatal area (SA), and stomatal relative area (SRA) were measured in different parts of wheat glumes from a doubled haploid (DH) population and their parents. Quantitative trait loci (QTLs) of these traits were anchored on a high-density genetic linkage map of the DH population. A total of 61 QTLs for stoma-related traits were mapped onto 16 chromosomes, and each one accounted for 3.63 to 19.02% of the phenotypic variations. Two QTL hotspots were found in two marker intervals, AX-109400932~AX-110985652 and AX-108972184~AX-108752564, on chromosome 6A. Five candidate genes (*TraesCS6A02G105400*, *TraesCS6A02G106400*, *TraesCS6A02G115100*, *TraesCS6A02G115400*, and *TraesCS6A02G116200*) were screened out, according to their expression levels in wheat glumes or spikes. The expression of these genes could be induced by a variety of abiotic stresses. These findings provide insights for cloning and functional characterization of stoma-related candidate genes in wheat glumes.

Quantitative trait loci mapping and candidate gene analysis of stoma-related traits in wheat (*Triticum aestivum* L.) glumes

Ning Li[1] Fanfan Dong[1] Tongtong Liu[2] Jinwen Yang[1] Yugang Shi[1] Shuguang Wang[1] Daizhen Sun[1] Ruilian Jing[3]

[1]College of Agronomy, Shanxi Agricultural University, Taigu, China
[2]College of Food Science and Engineering, Shanxi Agricultural University, Taigu, China
[3]National Key Facility for Crop Gene Resources and Genetic Improvement/Institute of Crop Sciences, Chinese Academy of Agricultural Sciences, Beijing, China

Corresponding author:
Daizhen Sun[1]
Mingxian South Road No.1, Taigu, 030801, Shanxi Province, China
Email address: e-mail: sdz64@126.com

Abstract

The photosynthesis of wheat glumes makes important contributions to the yield. Stomata play a crucial role in regulating photosynthesis and transpiration in plants. However, the genetic base of wheat glume stomata is not fully understood. In this study, stomatal length (SL), stomatal width (SW), stomatal density (SD), potential conductance index (PCI) of stomata, stomatal area (SA), and stomatal relative area (SRA) were measured in different parts of wheat glumes from a doubled haploid (DH) population and their parents. Quantitative trait loci (QTLs) of these traits were anchored on a high-density genetic linkage map of the DH population. A total of 61 QTLs for stoma-related traits were mapped onto 16 chromosomes, and each one accounted for 3.63 to 19.02% of the phenotypic variations. Two QTL hotspots were found in two marker intervals, AX-109400932~AX-110985652 and AX-108972184~AX-108752564, on chromosome 6A. Five candidate genes (*TraesCS6A02G105400*, *TraesCS6A02G106400*, *TraesCS6A02G115100*, *TraesCS6A02G115400*, and *TraesCS6A02G116200*) were screened out, according to their expression levels in wheat glumes or spikes. The expression of these genes could be induced by a variety of abiotic stresses. These findings provide insights for cloning and functional characterization of stoma-related candidate genes in wheat glumes.

Keywords: wheat (*Triticum aestivum* L.), glume, stomata, QTL, candidate gene

Introduction

Stomata are the main portals for the exchange of gas and water between plants and the external environment (*Li et al., 2017*), and they play an extremely important role in the life activities of plants. Plants can change their photosynthesis and transpiration rates through regulating the aperture, density, and distribution of stomata when they are stressed by biotic or abiotic factors (*Doheny-Adams et al., 2012*; *Franks et al., 2015*). In addition to spreading a large number on the leaves, stomata also exist on the epidermis of certain non-foliar organs, such as pods of soybean and oilseed rape, corn bracts, and ears of wheat. (*Wang et al., 2001*; *Kong et al., 2010*). &

Previous studies have reported that leaves are the main organs for plant photosynthesis to generate energy, and the photosynthesis of wheat flag leaves has always been regarded as the main source of assimilation during the filling process (*Maydup et al., 2010*). However, as scientists continue to deepen the research on plant photosynthesis, more and more results showed that the photosynthesis of plant non-foliar organs also plays an important role in the accumulation of carbon assimilates (*Sánchez-Díaz et al., 2002*; *Zhu et al., 2009*; *Sánchez-Bragado et al., 2014*). Compared with leaves, ear organs have unique advantages: for example, the photosynthetic products of wheat ears can be directly transported to the grain, thus avoiding unnecessary waste. Wheat ears carry out the C_4 metabolic pathway, which can re-fix the CO_2 produced by photorespiration (*Knoppik et al., 1986*; *Araus et al., 1993*). Wheat spikes have stronger drought tolerance, higher osmotic adjustment ability, and water use efficiency (WUE) (*Tambussi et al., 2005*). Compared with lower organs such as flag leaves, wheat spikes age more slowly (*Tambussi et al., 2007*). Thus, wheat ear photosynthesis also makes an important contribution to the yield (*Araus et al., 1993*; *Abbad et al., 2004*; *Zhou et al., 2014*).

Glumes are the main photosynthetic organs of the ear and are believed to be an important source of assimilates for kernel filling in wheat (*Araus et al., 1993*). Glumes can recycle the CO_2 respired by developing grains during photosynthesis and have higher ribulose-1,5-bisphosphate carboxylase (RuBPC, EC 4.1.1.39) activity compared with other ear elements (*Gebbing & Schnyder, 2001*; *Aliyev, 2012*; *Sánchez-Bragado et al.,* 2014). It has been reported that glumes actively participate in the process of CO_2 assimilation during kernel filling (*Lopes et al., 2006*). In addition, glumes maintain a higher relative water content and WUE under progressive water and dry stress than flag leaves, contributing significantly to grain filling (*Rubén et al., 2018*; *Wardlaw, 2002*). Therefore, compared with other organs, glumes may have a higher ability to resist abiotic stress.

So far, many reports on genetic analysis of stoma-related traits have focused on plant leaves, especially in rice. For example, *Teng et al.,* (2004) detected one QTL that controls the stomatal conductance of rice leaves at the peak tillering stage on chromosome 4. *Ishimaru et al.,* (2001) used a population of crosses between japonica and indica to detect a QTL that controls the stomatal density on the leaf surface and a QTL that is related to the stomatal density on the back of the leaf. Ten QTLs for stomatal density and four QTLs for stomatal size were detected across growth stages and leaf surfaces (adaxial and abaxial) (*Laza et al., 2010*). In wheat, twenty QTLs for stomatal density and size of leaves were identified under drought stress (*Wang et al., 2016*).

However, genetic analysis of stoma-related traits in spike organs is rarely reported.

In this study, stomatal density, length, and width on the top, middle, and base of wheat glumes were measured and the potential conductance index of stomata, stomatal area, and stomatal relative area in different parts of glumes were calculated. A high-density linkage genetic map was used for QTL mapping of stoma-related traits and the candidate genes related were screened. These QTLs and candidate genes will provide insights for studying the molecular mechanism of stomatal development of the wheat ear.

Materials & Methods

Test material

A wheat double haploid (DH) population (*Liu et al., 2013*), including 150 lines that derived from a cross between two Chinese winter wheat varieties, Hanxuan 10 (female parent, a variety with multiple abiotic stress tolerance) and Lumai 14 (male parent, a variety with high yield potential), was used in this study. All the 150 lines and parents were grown at the experimental farm (37°25′N, 112°35′E) of Shanxi Agricultural University in 2018 and 2019. The field experiments were conducted by randomized complete block design (RCBD) with three replicates. Each plot consisted of two rows of 2 m in length, with 0.25 m between rows. Water and fertilizer management during the growth period was complied with the local production practice.

Measurement and calculation of stomata-related traits in glumes

For each DH line and parents, three flowering plants with consistent growth were tagged. The middle spikes of the three plants were quickly placed into a 2-mL centrifuge tube with FAA solution (formalin: acetic acid: 70% alcohol = 1:1:18) 3 days after anthesis, respectively. Every tube was gently shaken, then stored at 4 ºC. After a spike was taken out, the glumes on both sides of each spikelet were removed. The surfaces of glumes were cleaned using a degreased cotton ball dipped in ethanol, and then carefully smeared with a thin film of nail varnish on the under epidermis. When dried, the film was peeled from the glume surface, mounted on a glass slide, and immediately covered with a cover slip. Five views were selected on the top, middle, and base of glumes, respectively. The number of stomata per view was scored, and stomatal length (SL) and stomatal width (SW) were measured under a 40X objective lens of a photomicroscope fitted with objective and eyepiece micrometers. Stomatal averages of five view areas ($S = \pi r^2$, r = view radius) were calculated, and stomatal density (SD) was defined as N/S (number of stomata per mm^2). Three stomata per view were randomly selected for measuring length and width, which were then meant as the value for each plant.

Calculations of other stoma-related traits were as follows:

Potential conductance index (PCI) = $SL^2 \times SD \times 10^{-4}$ (*Nicholas & Andrew, 2009*)

Stomatal area (SA) = $\pi \times 1/2$ SL $\times 1/2$ SW (*Robert et al., 2000*)

Stomatal relative area (SRA) = $SD \times SA \times 10^{-4}$ (*Sun et al., 2021*)

Data analysis

The relevant *t*-test and analysis of variance (ANOVA) were carried out by the statistical software

package SPSS v.17.0; the frequency distribution map was generated by Excel 2007; and the phenotypic correlation analysis map was created in the R-package corrplot (*Wei & Simko, 2013*).

QTL mapping

The genetic map of the DH population was constructed by Jing Ruilian's team at the Institute of Crop Science, Chinese Academy of Agricultural Sciences (*Li et al., 2019*). The linkage map is 4082.4 cM in length and contains 1630 SNP and 224 SSR markers, with 2.2 cM per bin on average (*Shi et al., 2020*). QTL mapping was performed based on the inclusive composite interval mapping method (*Li et al., 2008*) using the IciMapping 4.1 software with a 0.1-cM walking speed, and the likelihood of odds (LOD) threshold was set to 2.5 based on the results of 1000 permutations (*Li et al., 2021*).

Prediction of candidate genes and expression analysis

Candidate genes in associated loci were predicted according to the reference genome sequence of 'Chinese Spring' wheat (*IWGSC RefSeqv1.1*) published by the International Wheat Genome Sequencing Consortium. Gene annotation was carried out by referring to the Ensembl Plants database (https://plants.ensembl.org/index.html). We used a publicly available database, WheatOmics (http://wheatomics.sdau.edu.cn/) (*Ma et al., 2021*), to obtain the expression profiles of all candidate genes.

Results

Phenotypic variation of glume stoma-related traits in the DH population and parents

We observed regular rows of stomata on the top, middle, and base of glumes in parents (Fig. 1). SD of different parts of glumes in Lumai 14 showed significant or highly significant differences between the two years, while Hanxuan 10 had a significant difference in SD only at the base of glumes (Table 1). For DH lines, except for SD at the base of glumes, the phenotypic values of SD of other parts of glumes in 2019 were significantly lower than those in 2018 (Table 1). These results indicated that SD of glumes is greatly affected by the environment, and this phenomenon is more obvious in Lumai 14 than Hanxuan 10. In general, from the top to the base, SD of glumes gradually became smaller (Table 1).

Except for the middle of glumes in Hanxuan10, differences in SL of the rest parts of glumes between the two years were not significant in the two parents. Except for the top of glumes of Lumai 14, differences in SW of the rest parts of glumes between the two years were not significant in the two parents. For the DH lines, the difference in SL of glumes was not significant between the two years, but SW in 2019 was highly significantly smaller than that in 2018 (Table 1). These results indicated that SW of glumes is more affected by the environment than SL.

Except for the middle of glumes of Lumai 14, differences in stomatal PCI of the rest parts of glumes between the two years were not significant in the two parents. Differences in stomatal PCI of all parts between the two years were not significant for the DH lines neither. Differences in SA of all parts between the two years were not significant in the two parents. Except for the

top and middle of glumes of Lumai 14, differences in SRA of the rest parts of glumes between the two years were not significant in the two parents (Table 1).

Stoma-related traits of the DH lines showed showed continuous transgressive segregation with skewness and kurtosis values close to zero, suggesting normal distribution. All target traits were thus quantitatively controlled by multiple genes and were suitable for QTL mapping (Table 1) (Fig. S1).

Correlation between glume stoma-related traits

For all parts of glumes, SD showed a highly significantly negative correlation with SL in 2018 and 2019; however, the correlation between SD and SW was not significant. There was a significantly or highly significantly positive correlation between SL and SW in 2018, but such correlation was not significant in 2019. In addition, SD showed a highly significantly positive correlation with PCI and SRA in 2018 and 2019. SL showed a significantly positive correlation with SA in both years. SW showed a significantly positive correlation with SA and SRA in both years. In 2018, any two of PCI, SA, and SRA were significantly positively correlated, while the degree of correlation was weakened in 2019(Fig. 2 Table S1).

QTL mapping for traits related to stomata in wheat glumes

A total of 61 QTLs for traits related to stomata of wheat glumes were detected in the two years. The phenotypic variation of these QTLs ranged from 3.63 to 19.02%. The LOD score ranged from 2.51 to 22.12, and the QTLs were distributed on 16 chromosomes including 1A, 1D, 2A, 2B 2D, 3A, 3D, 4B, 5A, 5B, 5D, 6A, 6B, 7A, 7B, and 7D, respectively (Fig.3 Table 2).

A total of 10 QTLs corresponding to SD of glumes were detected in the two years. The phenotypic variation of these QTLs ranged from 6.78 to 11.41%. Among these QTLs, *QSDt-2A* was detected in both years; *QSDt-5A* and *QSDm-5A* were detected in the same interval in 2018. Twenty-one QTLs were associated with stomatal size and detected in both years. Among these QTLs, *QSLt-2D*, *QSLm-7A*, and *QSLb-6A-1* were detected in both years. *QSLb-6A-2* and *QSWb-6A* were detected in the same interval in 2019. A total of 30 QTLs associated with PCI, SA, and SRA were detected in the two years. Among these QTLs, *QPCIb-6A-1*, *QSAt-2D*, *QSAm-3A*, and *QSRAb-6A-2* were detected in the two years. Among all QTLs, *QSRAb-6A-1* had the largest effect explaining 22.12% of the total phenotypic variation (Fig.3 Table 2).

Among all QTLs, two QTL hotspots were found on chromosome 6A. One was in the interval AX-109400932~AX-110985652, which contained four QTLs related to SL, SD, PCI, and SRA in the two years. The other was in the interval AX-108972184~AX-108752564, which contained four QTLs related to SW, SD, PCI, and SRA in the two years (Fig.3 Table 2).

Expression analyses of candidate genes

For the first QTL hotspot, the physical positions of the two markers AX-109400932 and AX-110985652 were 73571398 and 76990896 bp, respectively. According to the reference genome sequence of 'Chinese Spring' wheat (*IWGSC RefSeqv1.1*), a total of 33 genes were found between the two markers, and gene annotation was carried out by referring to the Ensembl Plants database (Table S2). For the other QTL hotspot, the physical positions of the two markers AX-108972184 and AX-108752564 were 83931623 and 86272494 bp, respectively, and a total of 24

genes were found between these two markers (Table S2). Using WheatOmics, the expression levels of these 57 genes in wheat glumes and spikes were predicted (*IWGSC et al., 2018*). The results showed that there were five genes (*TraesCS6A01G105400*, *TraesCS6A01G106400*, *TraesCS6A01G115100*, *TraesCS6A01G115400*, and *TraesCS6A01G116200*) with higher expression levels in wheat glumes or spikes (Fig.4 Table 3).

Then, the expression levels of these five genes under different abiotic stresses were analyzed (*Oono et al., 2013*; *Liu et al., 2015*; *Nazanin et al., 2019*). The results showed that the expression of these genes was induced by different abiotic stresses, and the expression patterns of different genes under the same abiotic stress were also different (Fig. 5). For example, the expression of *TraesCS6A01G105400* was significantly reduced after being subjected to low phosphorus stress in wheat shoots and roots. The expression levels of *TraesCS6A01G115100* and *TraesCS6A01G116200* both increased after being subjected to low phosphorus stress in shoots and roots. The expression of *TraesCS6A01G106400* was only significantly increased in the root after being subjected to low phosphorus stress. The expression level of *TraesCS6A01G105400* was significantly reduced in wheat seedling leaves subjected to drought stress, heat stress, and their combination. The expression levels of *TraesCS6A01G106400* and *TraesCS6A01G116200* were significantly increased after six hours of drought stress, heat stress, and their combination. Among these five genes, only the expression level of *TraesCS6A01G115400* was significantly decreased after being exposed to salt stress (Fig. 5).

Discussion

Phenotypic correlation of stoma-related traits in wheat glumes

Stomata are the channel for water and gas exchange in the process of wheat photosynthesis and respiration, which indirectly affect the yield of wheat (*Berger et al., 2000*). Studies have shown that a variety of environmental factors at different growth and developmental stages of plants can affect the formation of stomata, such as water (*Stephens et al., 2017*), temperature (*Qi et al., 2018*), light (*Boccalandro et al., 2009*), and CO_2 concentration (*Hu et al., 2010*). *Aasamaa et al.,* (2001) reported that the stomatal length of forest tree species decreased with increasing drought. For some light-loving crops, the formation of stomata can be promoted by increasing the light intensity. In the present study, stomatal density and stomatal width of wheat glumes showed significant differences between the two years, but stomatal length showed no significant differences (Table 1). These results suggest that stomatal length may have higher stability in response to different environmental conditions than stomatal density and width.

Franks and Beerling (2009) have shown that the negative correlation between stomatal size and stomatal density helps to adjust the plasticity of stomata, thereby regulating the maximal stomatal conductance of wheat. There was a significantly negative correlation between stomatal density and stomatal size in wheat leaves (*Wang et al., 2016*). In addition, similar phenomena have been observed in other crops. (*Ishimaru et al., 2001*; *Ohsumi et al., 2007*). The present results showed that stomatal density was negatively correlated with stomatal length in each part of wheat glumes in the two years. However, there was no significant correlation between

stomatal density and stomatal width. Previous studies found that stomatal length and stomatal width in wheat leaves were significantly positively correlated (*Wang et al., 2016*). The present results showed that stomatal length and stomatal width were significantly positively correlated in 2018 (Fig. 2 Table S1). Therefore, wheat glumes can improve their adaptability to different environmental conditions by coordinating the relationship among stomatal density, stomatal length, and stomatal width.

Pleiotropy of QTLs for stoma-related traits in wheat

Various studies have found that QTLs of closely related traits may be located on the same or nearby positions on the chromosomes (*Fracheboud et al., 2002*; *Tuberosa et al., 2002*). In the present study, *QSLb-6A*-1 corresponding to stomatal length at the base of glumes, *QSDb-6A* for stomatal density at the base of glumes, *QPCIb-6A-1* for stomatal PCI at the base of glumes, and *QSRAd-6A-1* for stomatal relative area at the base of glumes were detected in the interval of AX-109400932~AX-110985652 on chromosome 6A in 2018 and 2019. In the vicinity of this interval, *QSWb-6A*, *QSLb-6A*-2, *QPCIb-6A*-2, and *QSRAb-6A*-2 were detected in the interval AX-108972184~AX-108752564 on chromosome 6A in the two years. *QSDt-5A*, *QSDm-5A*, and *QSRAt-5A* were all located in the interval AX-111662464~AX-95683796. *QSDt-5D* and *QSLt-5D* were located in the interval Xgwm205.2~AX-89390905. *QSDm-1A* and *QSLt-1A* were located in the interval AX-111105973~AX-94402739 (Fig. 3 Table 2).

In addition, compared with previous studies, we found a QTL *QSWt-4B* in this study was located within the region of *QAGsw4B* in the previous study (*Wang et al., 2018*). *QSAb-5A-2* was located within the region of *QAGsd5A*, *QMGsd5A-2*, and *QAGsl5A*. (*Wang et al., 2018*). *QSRAm-5B* was located close to the region of *QPsd5B*, and *QSDd-5A* was located within the region of *QSD5A-2* (*Wang et al., 2016*).

Therefore, the QTLs for above-mentioned stoma-related traits, which were detected in different parts of wheat, different growth periods, and various environments, were significant markers for stoma-related traits in wheat. Furthermore, these findings implied stomatal density and size of wheat leaves and glumes may be controlled by the same or pleiotropic genes. The markers that were localized within a QTL interval associated with stoma-related traits not only validated the QTL but also provided more closely linked markers. These markers will be useful to reveal advanced wheat varieties in wheat breeding programs based on marker-assisted selection approaches.

Prediction of candidate genes related to stomata in wheat glumes

In this study, 57 genes were found in two intervals, AX-109400932~AX-110985652 (physical range 73571398-76990896 bp) and AX-108972184~AX-108752564 (physical range 83931623-86272494 bp), on chromosome 6A, and five candidate genes (i.e., *TraesCS6A01G105400*, *TraesCS6A01G106400*, *TraesCS6A02G115100*, *TraesCS6A02G115400*, and *TraesCS6A02G116200*) were screened out, according to their expression levels in wheat glumes or spikes (Fig. 4 Table 3).

The expression level of *TraesCS6A01G105400* in wheat glumes and spikes was the highest among all candidate genes (Fig. 4), and its functional annotation was 50S ribosomal protein L3

(Table 3). The *TraesCS6A01G105400* expression decreased significantly under low phosphorus, drought, and heat stress conditions (Fig. 5). The functional annotation of the candidate gene *TraesCS6A01G106400* is stress-associated endoplasmic reticulum (ER) protein (Table 3). The ER plays a crucial role in the maintenance of cellular homeostasis. ER stress is a widely existed stress mechanism to external stimuli in plants and animals. This pathway maintains the ER homeostasis and alleviates stress damage through regulation of a series of gene expressions (*Park & Park, 2019*). The expression of *TraesCS6A01G106400* was significantly increased under salt stress (Fig. 5). The functional annotation of the candidate gene *TraesCS6A01G115100* is purple acid phosphatase (PAP) (Table 3), and its expression was significantly increased under low phosphorus stress (Fig. 5). PAPs are members of the metallo-phosphoesterase family identified from a wide range of plants. PAPs have mostly been studied for their potential involvement in phosphorus acquisition and redistribution because of their ability to catalyze the hydrolysis of activated phosphate esters and anhydrides under acidic conditions (*Olczak et al., 2003*). Recent studies also showed that PAPs play important roles in modulating plant carbon metabolism, cell wall synthesis, pathogen resistance, etc (*Kaida et al., 2009*; *Sun et al., 2012*; *Zhang et al., 2014*). *TraesCS6A01G115400* was specifically expressed in wheat glumes, and its functional annotation is calcium-dependent lipid-binding family protein (Table 3). Ca^{2+} is a second messenger in plants that regulates virtually all aspects of plant development and responses to environmental stimuli. Ca^{2+} usually tends to rapidly rise under abiotic stresses (*Bartels & Sunkar, 2005*). Several proteins have been reported to be activated or translocated in the presence of Ca^{2+} including Calcium-dependent lipid-binding protein (*Hurley & Misra, 2000*). The expression of *TRAESCS6A01G115400* in roots of wheat seedlings was significantly decreased under salt stress (Fig. 5). The functional annotation of the candidate gene *TraesCS6A01G116200* is ATP-dependent RNA helicase (Table 3). ATP-dependent RNA helicase can be found in many organisms, which is involved in the multi-dimensional metabolism of RNA and plays an important role in plant growth and development, especially in abiotic stress response (*Kim et al., 2008*). The expression of *TraesCS6A01G116200* was significantly increased under low phosphorus, drought, and heat stress (Fig. 5).

The above 5 candidate genes not only had high expression levels in wheat glumes or spikes, but are also induced by a variety of abiotic stresses. Studies have shown that when plants are subjected to abiotic stress, they can change their photosynthetic rate and transpiration rate by adjusting the stomata size, stomata density, and stomata distribution to deal with bad external environments (*Doheny-Adams et al., 2012*; *Franks et al., 2015*). Therefore, it will be greatly helpful to analyze whether these five genes affect the formation of wheat stomata through transgenic experiments in future research, and to explore the mechanism of their functions.

Conclusion

In this study, a total of 61 QTLs for traits related to stomata of wheat glumes were identified in the two years, which were distributed across 16 chromosomes and explained 3.63-19.02% of phenotypic variation. Among them, two QTL hotspots were found in 6A, including four and four QTLs, respectively. Subsequently, five candidate genes were screened out, according to their

expression levels in wheat glumes or spikes. The expression of these genes could be induced by a variety of abiotic stresses. Our results provide insights for cloning and functional characterization of stoma-related candidate genes in wheat glumes.

ADDITIONAL INFORMATION AND DECLARATIONS

Acknowledgments

We gratefully acknowledge the anonymous reviewers for their constructive comments. We would also like to thank TopEdit (www.topeditsci.com) for its linguistic assistance during the preparation of this manuscript.

Funding

This work was funded by Science & Technology Innovation Foundation of Shanxi Agricultural University (2020BQ30), Outstanding Doctor Funding Award of Shanxi Province (SXYBKY2019040).

Competing Interests

The authors declare that they have no competing interests

Data Availability

All data generated or analyzed during this study are included in this published article.

References

Aasamaa K, Sober A, Rahi M. 2001. Leaf anatomical characteristics associated with shoot hydraulic conductance, stomatal conductance, and stomatal sensitivity to changes of leaf water status in temperate deciduous trees. *Australia Journal of Plant Physiology* **28**: 765-774.

Abbad H, Jaafari SE, Bort J, Araus JL. 2004. Comparison of flag leaf and ear photosynthesis with biomass and grain yield of durum wheat under various water conditions and genotypes. *Agronomie* **24**: 19-28.

Aliyev JA. 2012. Photosynthesis, photorespiration and productivity of wheat and soybean genotypes. *Physiologia Plantarum* **145**: 369-383.

Araus JL, Bort J, Brown HR, Bassett C, Cortadellas N. 1993. Immunocytochemical localization of phosphoenolpyruvate carboxylase and photosynthetic gas exchange characteristics in ears of *Triticum durum* Desf. *Planta* **191**: 507-514.

Bartels D, Sunkar R. 2005. Drought and salt tolerance in plants. *Critical Reviews in Plant Sciences* **24**: 23-58.

Berger D, Altmann T. 2000. A subtilisin-like serine protease involved in the regulation of stomatal density and distribution in Arabidopsis thaliana. *Genes and Development* **14**: 1119-

1131.

Boccalandro HE, Rugnone ML, Moreno JE, Ploschuk EL, Serna L, Yanovsky MJ, Casal JJ. 2009. Phytochrome b enhances photosynthesis at the expense of water-use efficiency in Arabidopsis. *Plant Physiology* **150**: 1083-1092.

Doheny-Adams T, Hunt L, Franks PJ, Beerling DJ, Gray JE. 2012. Genetic manipulation of stomatal density influences stomatal size, plant growth and tolerance to restricted water supply across a growth CO_2 gradient. *Philosophical Transactions of the Royal Society B: Biological Sciences* **367**:547-555.

Fracheboud Y, Ribaut JM, Vargas M, Mesamer R, Stamp P. 2002. Identification of quantitative trait loci for cold tolerance of photosynthesis in maize (*Zea mays* L.). *Journal of Experimental Botany* **53**:1967-1977.

Franks PJ, Beerling DJ. 2009. Maximum leaf conductance driven by CO_2 effects on stomatal size and density over geologic time. *Proceedings of the National Academy of Sciences* **106**:10343-10347.

Franks PJ, Doheny-Adams TW, Britton-Harper ZJ, Gray JE. 2015. Increasing water-use efficiency directly through genetic manipulation of stomatal density. *New Phytologist* **207**:188-195.

Gebbing T, Schnyder H. 2001. 13C Labeling kinetics of sucrose in glumes indicates significant refixation of respiratory CO_2 in the wheat ear. *Functional Plant Biology* **28**:1047-1053.

Hu HH, Boisson-Dernier A, Israelsson NM, Böhmer M, Xue SW, Ries A, Godoski J, Kuhn JM, Schroeder JI. 2010. Carbonic anhydrases are upstream regulators in guard cells of CO_2-controlled stomatal movements. *Nature Cell Biology* **12**:87-93.

Hurley JH, Misra S. 2000. Signaling and subcellular targeting by membrane-binding domains. *Annual Review of Biophysics and Biomolecular Structure* **29**:49-79.

Ishimaru K, Shirota K, Higa M, Kawamitsu Y. 2001. Identification of quantitative trait loci for adaxial and abaxial stomatal frequencies in *Oryza sativa*. *Plant Physiology and Biochemistry* **39**:173-177.

Kaida R, Satoh Y, Bulone V, Yamada Y, Kaku T, Hayashi T, Kaneko TS. 2009. Activation of β-glucan synthases by wall-bound purple acid phosphatase in tobacco cells. *Plant Physiology* **150**:1822-1830.

Kim JS, Kim KA, Oh TR, Park CM, Kang H. 2008. Functional characterization of DEAD-box RNA helicases in Arabidopsis thaliana under abiotic stress conditions. *Plant and Cell Physiology* **49**:1563-1571.

Knoppik D, Selinger H, Ziegler-Jöns A. 1986. Differences between the flag leaf and of ear of a spring wheat cultivar (*Triticum aestivum* cv. Arkas) with respect to the CO_2 response of assimilation, respiration and stomatal conductance. *Physiologia Plantarum* **68**:451-457.

Kong LA, Wang FH, Feng B, Li SD, Si JS, Zhang B. 2010. The structural and photosynthetic characteristics of the exposed peduncle of wheat (*Triticum aestivum* L.)*:* an important photosynthate source for grain-filling. *BMC Plant Biology*, **10**: 141.

Laza MRC, Kondo M, Ideta O, Barlaan E. Imbe T. 2010. Quantitative trait loci for stomatal density and size in lowland rice. *Euphytica.* **172**:149-158.

Li HH, Ribaut JM, Li ZL, Wang JK. 2008. Inclusive composite interval mapping (ICIM) for digenic epistasis of quantitative traits in biparental populations. *Theoretical and Applied Genetics*, **116**:243-260.

Li L, Peng Z, Mao XG, Wang JY, Li CN, Chang XP, Jing RL. 2021. Genetic insights into natural variation underlying salt tolerance in wheat. *Journal of Experimental Botany*, **72**:1135-1150.

Li L, Mao XG, Wang JY, Chang XP, Reynolds M, Jing RL. 2019. Genetic dissection of drought and heat-responsive agronomic traits in wheat. *Plant Cell and Environment*, **42**:2540-2553.

Li YP, Li HB, Li YY, Zhang SQ. 2017. Improving water-use efficiency by decreasing stomatal conductance and transpiration rate to maintain higher ear photosynthetic rate in drought-resistant wheat. *The Crop Journal*, **5**:231-239.

Liu XL, Li RZ, Chang XP, Jing RL. 2013. Mapping QTLs for seedling root traits in a doubled haploid wheat population under different water regimes. *Euphytica*, **189**:51-66.

Liu ZS, Xin MM, Qin XJ, Peng HR, Ni ZF, Yao YY, Sun QX. 2015. Temporal transcriptome profiling reveals expression partitioning of homeologous genes contributing to heat and drought acclimation in wheat (*Triticum aestivum* L.). *BMC Plant Biology*, **15**:152.

Lopes MS, Cortadellas N, Kichey T, Dubois F, Habash DZ, Araus JL. 2006. Wheat nitrogen metabolism during grain filling: comparative role of glumes and the flag leaf. *Planta,* **225**:165-181.

Ma SW, Wang M, Wu JH, Guo WL, Chen YM, Li GW, Wang YP, Shi WM, Xia GM, Fu DL, Kang ZS, Ni F. 2021. WheatOmics: a platform combining multiple omics data to accelerate functional genomics studies in wheat. Mol Plant ***14***:1965-1968.

Maydup ML, Antonietta M, Guiamet JJ, Graciano C, López JR, Tambussi EA. 2010. The contribution of ear photosynthesis to grain filling in bread wheat (*Triticum aestivum* L.). *Field Crops Research* **119**:48-58.

Nazanin A, Ahmad I, Mohammad RG, Farhad NF, Shobbar ZS. 2019. Transcriptome response of roots to salt stress in a salinity-tolerant bread wheat cultivar. *PLoS ONE* **14**: 3.

Nicholas H, Richardson AD. 2009. Stomatal length correlates with elevation of growth in four temperate species. *Journal of Sustainable Forestry* **28**:63-73.

Ohsumi A, Kanemura T, Homma K, Horie T, Shiraiwa T. 2007. Genotypic variation of stomatal conductance in relation to stomatal density and length in rice (*Oryza sativa* L.). *Plant Production Science* **10**:322-328

Qi X, Torii KU. 2018. Hormonal and environmental signals guiding stomatal development. *BMC Biology* **16**:21.

Olczak M, Morawiecka B, Watorek W. 2003. Plant purple acid phosphatases-genes, structures and biological function. *Acta Biochimica Polonica* **50**:1245-1256.

Oono Y, Kobayashi F, Kawahara Y, Yazawa T, Handa H, Itoh T, Matsumoto T. 2013. Characterisation of the wheat (triticum aestivum L.) transcriptome by de novo assembly for the discovery of phosphate starvation-responsive genes: gene expression in Pi-stressed wheat. *BMC Genomics* **14**:77.

Park CJ, Park JM. 2019. Endoplasmic reticulum plays a critical role in integrating signals generated by both biotic and abiotic stress in plants. *Frontiers in Plant Science* **10**:399.

Robert RW, Gretchen FS, Richard GP. 2000. A comparison of leaf anatomy in field-grown gossypium hirsutum and G. barbadense. *Annals of Botany* **86**: 731-738.

Rubén V, Omar V D, Susan M, Fadia C, Shawn CK, Jordi B, María DS, Nieves A, José LA. 2018. Durum wheat ears perform better than the flag leaves under water stress: gene expression and physiological evidence. *Environmental and Experimental Botany* **153**:271-285.

Sánchez-Bragado R, Molero G, Reynolds MP, Araus JL. 2014. Relative contribution of shoot and ear photosynthesis to grain filling in wheat under good agronomical conditions assessed by differential organ $\delta^{13}C$. *Journal of Experimental Botany* **65**: 5401-5413.

Sánchez-Díaz M, García JL, Antolín MC, Araus JL. 2002. Effects of soil drought and atmospheric humidity on yield, gas exchange, and stable carbon composition of barley. *Photosynthetica* **40**: 415-421.

Shi HW, Guan WH, Shi YG, Wang SG, Fan H, Yang JW, Chen WG, Zhang WJ, Sun DZ, Jing RL. 2020. QTL mapping and candidate gene analysis of seed vigor-related traits during artificial aging in wheat (*Triticum aestivum*). *Scientific reports* **10**: 22060.

Stephens J, Waugh R. 2017. Reducing stomatal density in barley improves drought tolerance without impacting on yield. *Plant Physiology* **174**: 776-787.

Sun F, Suen PK, Zhang Y, Sun F, Suen PK, Zhang YJ, Liang C, Carrie C, Whelan J, Ward JL, Hawkins ND, Jiang LW, Lim BL. 2012. A dual-targeted purple acid phosphatase in Arabidopsis thaliana moderates carbon metabolism and its overexpression leads to faster plant growth and higher seed yield. *New Phytologist* **194**:206-219.

Sun JG, Liu CC, Hou JH, He NP. 2021. Spatial variation of stomatal morphological traits in grassland plants of the Loess Plateau. *Ecological Indicators* **128**:107857.

Tambussi EA, Bort J, Guiamet JJ, Nogués S, Araus JL. 2007. The Photosynthetic Role of Ears in C3 Cereals: Metabolism, Water Use Efficiency and Contribution to Grain Yield. *Critical Reviews in Plant Sciences* **26**: 1-16.

Tambussi E, Nogues SJ. 2005. Ear of durum wheat under water stress: water relations and photosynthetic metabolism. *Planta* **221**:446-458.

Teng S, Qian Q, Zeng DL, Kunihiro Y, Fujimoto K, Huang DN, Zhu LH. 2004. QTL analysis of leaf photosynthetic rate and related physiological traits in rice (*Oryza sativa* L.). *Euphytica* **135**: 1-7.

The International Wheat Genome Sequencing Consortium (IWGSC). 2018. Shifting the limits in wheat research and breeding using a fully annotated reference genome. *Science* **361**: eaar7191.

Tuberosa R, Salvi S, Sanguineti MC, Landi P, Maccaferri M, Conti S. 2002. Mapping QTL regulating morphophysiologyical traits and yield: Case studies, shortcomings and perspectives in drought stressed maize. *Annals of Botany* **89**:941-963.

Wang ZM, Wei AL, Zheng DM. 2001. Photosynthetic characteristics of non-leaf organs of

winter wheat cultivars differing in ear type and their relationship with grain mass per ear. *Photosynthetica* **39**: 239-244.

Wang SG, Dong FF, Sun DZ, Chen YY, Yan X, Jing RL. 2018. QTL analysis for stomatal density and size in wheat spike organ. *Emirates Journal of Food and Agriculture* **30**: 173-179.

Wang SG, Jia SS, Sun DZ, Fan H, Chang XP, Jing RL. 2016. Mapping QTLs for stomatal density and size under drought stress in wheat (*Triticum aestivum* L.). *Journal of Integrative Agriculture* **9**: 1955-1967.

Wardlaw IF. 2002. Interaction between drought and chronic high temperature during kernel filling in wheat in a controlled environment. *Annals of Botany* **90**: 469-476.

Wei TY, Simko V. 2013. Corrplot: visualization of a correlation matrix. *MMWR Mmwr Morbidity and Mortality Weekly Report* **52**: 145-151.

Zhang YJ, Sun F, Fettke J, Schöttler MA, Ramsden L, Fernie AR, Lim BL. 2014. Heterologous expression of AtPAP2 in transgenic potato influences carbon metabolism and tuber development. *FEBS Letters* **588:** 3726-3731.

Zhou BW, Sanz-Sáez Á, Elazab A, Shen TM, Sánchez-Bragado R, Bort J, Serret DM, Araus JL. 2014. Physiological traits contributed to the recent increase in yield potential of winter wheat from Henan Province, China. *Journal of Integrative Plant Biology* **56**: 492-504.

Zhu CX, Zhu JG, Zeng Q, Liu G, Xie ZB, Tang HY, Cao JL, Zhao XZ. 2009. Elevated CO^2 accelerates flag leaf senescence in wheat due to ear photosynthesis which causes greater ear nitrogen sink capacity and ear carbon sink limitation. Funct. *Plant Biology* **36**: 291-299.

Figure 1 Distribution of stomata in different parts of wheat glumes observed in 2018 (a) and 2019 (b).

Figure 2 Correlation of stoma-related traits in 2018 (a) and 2019 (b). Red and blue colors indicate significantly positive and negative correlations, respectively, whereas white color indicates no significant correlation. SD, stomatal density; SL, stomatal length; SW, stomatal width; PCI, potential conductance index; SA, stomatal area; SRA, stomatal relative area; t, top of glumes; m, middle of glumes; b, base of glumes

Figure 3 Distribution of QTLs for stoma-related traits on a high-density linkage map. To better display the QTLs, the high-density linkage maps show only markers near the QTL intervals. The QTLs with red fonts indicates that they were detected in both years

Figure 4 The locations of two QTL hotspots on chromosome and the candidate genes contained in the two regions. (a) LOD value of each traits. The line indicates the position where LOD is equal to 2.5. SD, stomatal density; SL, stomatal length; SW, stomatal width; PCI, potential conductance index; SRA, stomatal relative area; b, base of glumes. (b) Heat maps of expression of candidate genes contained in the two regions in wheat spikelets and glumes. The

five genes below the red arrow are candidate genes that were screened out in this study

Figure 5 Expression of candidate genes under various abiotic stresses. (a) low phosphorus stress; (b) drought and heat stress; (c) salt stress

Figure S1 Frequency distribution of stoma-related traits of wheat glumes in DH population. SD, stomatal density; SL, stomatal length; SW, stomatal width; PCI, potential conductance index; SA, stomatal area; SRA, stomatal relative area; t, top of glumes; m, middle of glumes; b, base of glumes.

Figure 1

Distribution of stomata in different parts of wheat glumes observed in 2018 (a) and 2019 (b) .

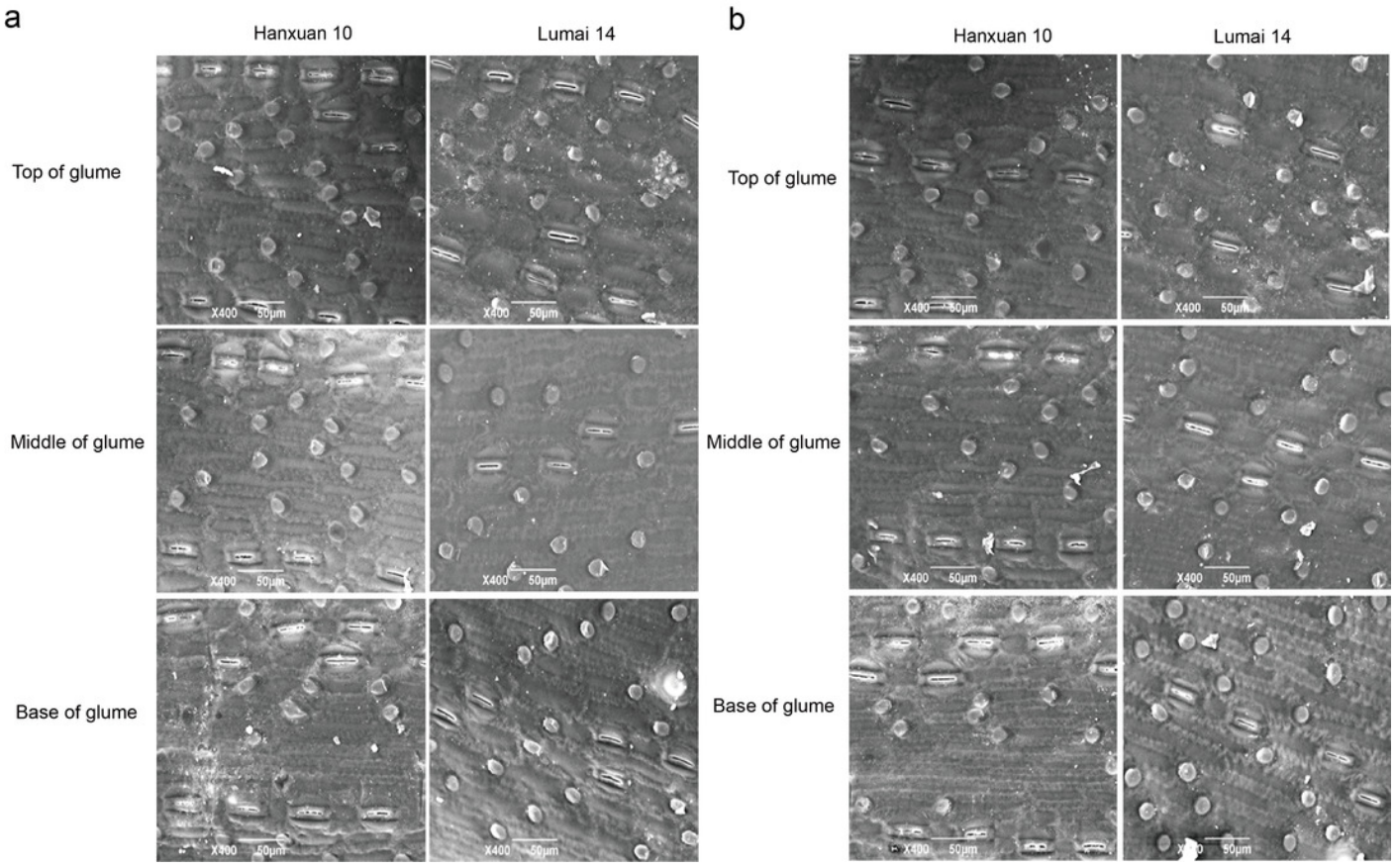

Figure 2

Correlation of stoma-related traits in 2018 (a) and 2019 (b).

R ed and blue colors indicate significantly positive and negative correlations, respectively, whereas white color indicates no significant correlation. SD, stomatal density; SL, stomatal length; SW, stomatal width; PCI, potential conductance index; SA, stomatal area; SRA, stomatal relative area; t, top of glumes; m, middle of glumes; b, base of glumes

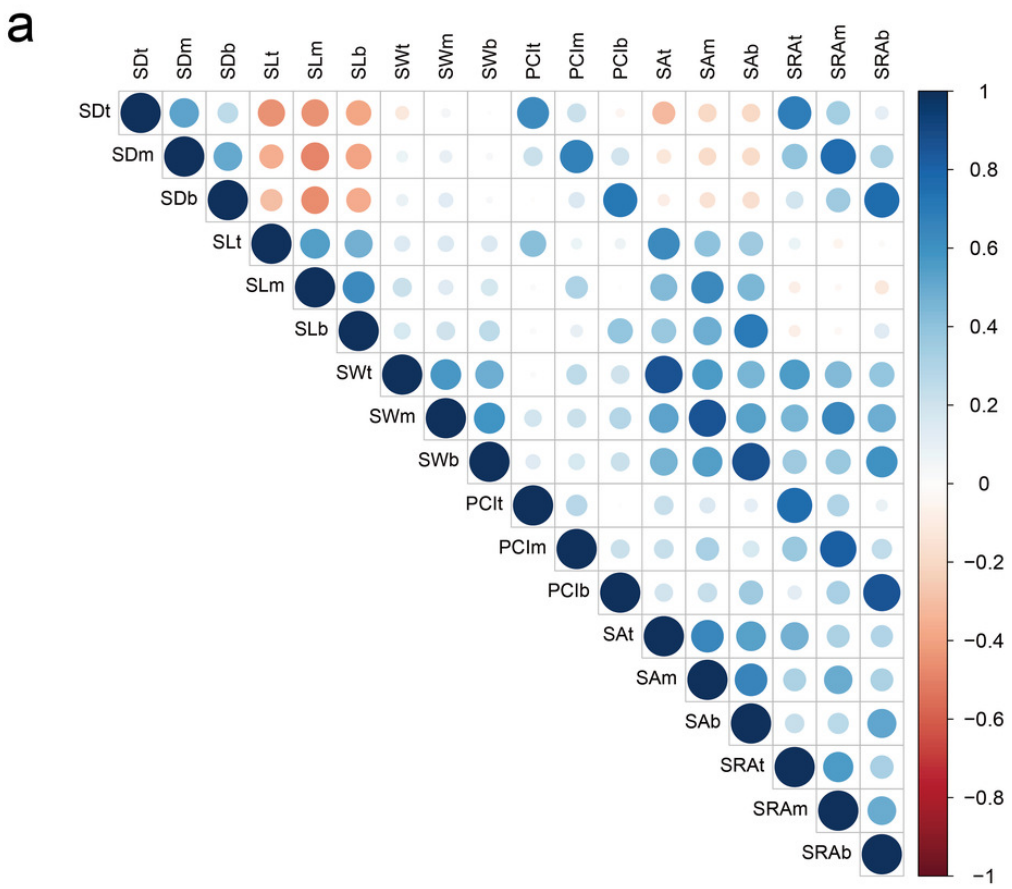
a
SDt
SDm
SDb
SLt
SLm
SLb
SWt
SWm
SWb
PCIt
PCIm
PCIb
SAt
SAm
SAb
SRAt
SRAm
SRAb
1
0.8
0.6
0.4
0.2
0
−0.2
−0.4
−0.6
−0.8
−1

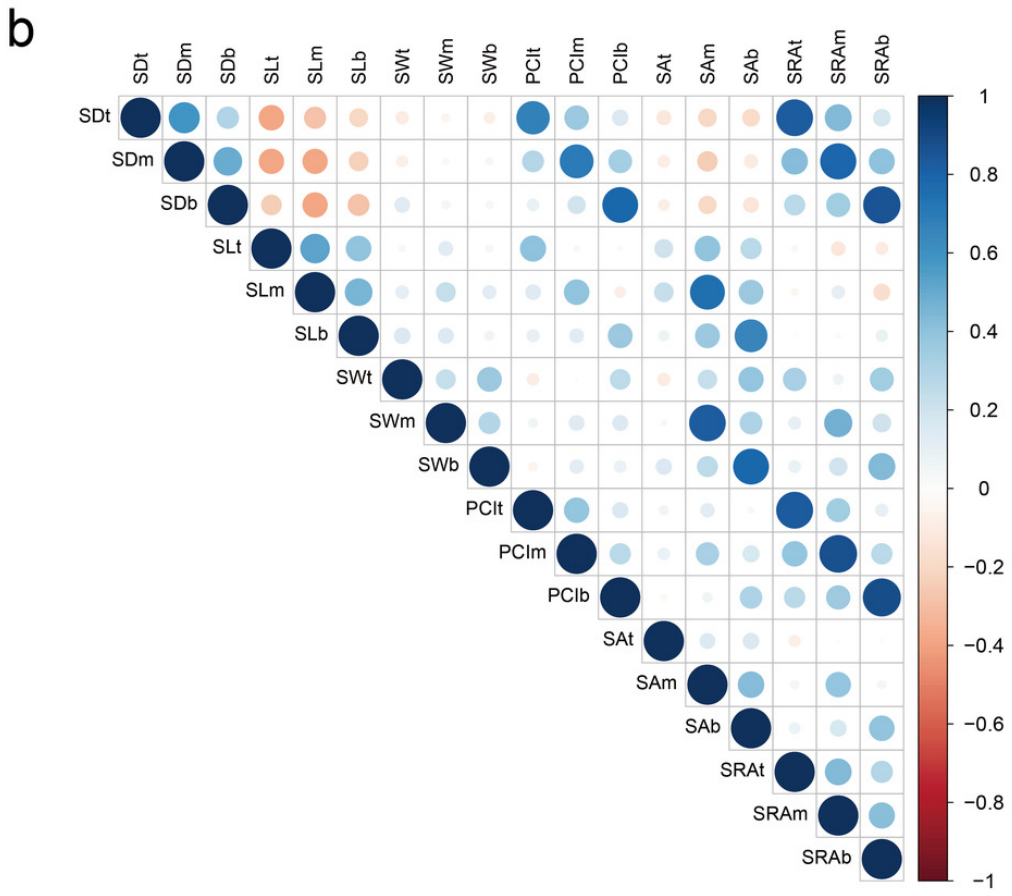
b
SDt
SDm
SDb
SLt
SLm
SLb
SWt
SWm
SWb
PCIt
PCIm
PCIb
SAt
SAm
SAb
SRAt
SRAm
SRAb
1
0.8
0.6
0.4
0.2
0
−0.2
−0.4
−0.6
−0.8
−1

Figure 3

Distribution of QTLs for stoma-related traits on a high-density linkage map.

To better display the QTLs, the high-density linkage maps show only markers near the QTL intervals. The QTLs with red fonts indicates that they were detected in both years

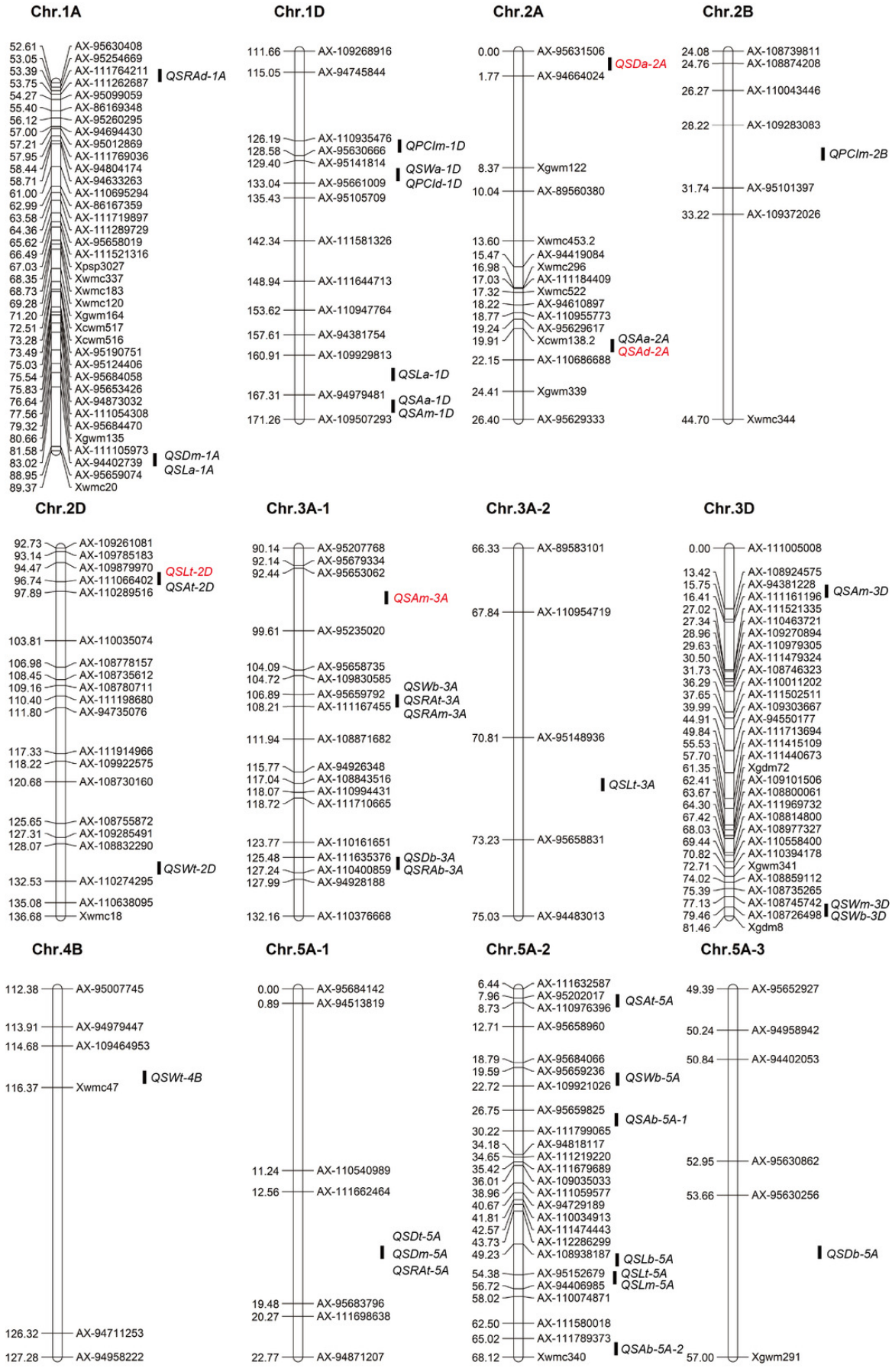
Chr.1A
52.61 AX-95630408
53.05 AX-95254669
53.39 AX-111764211
53.75 AX-111262687 QSRAd-1A
54.27 AX-95099059
55.40 AX-86169348
56.12 AX-95260295
57.00 AX-94694430
57.21 AX-95012869
57.95 AX-111769036
58.44 AX-94804174
58.71 AX-94633263
61.00 AX-110695294
62.99 AX-86167359
63.58 AX-111719897
64.36 AX-111289729
65.62 AX-95658019
66.49 AX-111521316
67.03 Xpsp3027
68.35 Xwmc337
68.73 Xwmc183
69.28 Xwmc120
71.20 Xgwm164
72.51 Xcwm517
73.28 Xcwm516
73.49 AX-95190751
75.03 AX-95124406
75.54 AX-95684058
75.83 AX-95653426
76.64 AX-94873032
77.56 AX-111054308
79.32 AX-95684470
80.66 Xgwm135
81.58 AX-111105973 QSDm-1A
83.02 AX-94402739 QSLa-1A
88.95 AX-95659074
89.37 Xwmc20
Chr.1D
111.66 AX-109268916
115.05 AX-94745844
126.19 AX-110935476 QPCIm-1D
128.58 AX-95630666
129.40 AX-95141814 QSWa-1D
133.04 AX-95661009 QPCId-1D
135.43 AX-95105709
142.34 AX-111581326
148.94 AX-111644713
153.62 AX-110947764
157.61 AX-94381754
160.91 AX-109929813 QSLa-1D
167.31 AX-94979481 QSAa-1D
171.26 AX-109507293 QSAm-1D
Chr.2A
0.00 AX-95631506 QSDa-2A
1.77 AX-94664024
8.37 Xgwm122
10.04 AX-89560380
13.60 Xwmc453.2
15.47 AX-94419084
16.98 Xwmc296
17.03 AX-111184409
17.32 Xwmc522
18.22 AX-94610897
18.77 AX-110955773
19.24 AX-95629617
19.91 Xcwm138.2 QSAa-2A QSAd-2A
22.15 AX-110686688
24.41 Xgwm339
26.40 AX-95629333
Chr.2B
24.08 AX-108739811
24.76 AX-108874208
26.27 AX-110043446
28.22 AX-109283083
QPCIm-2B
31.74 AX-95101397
33.22 AX-109372026
44.70 Xwmc344
Chr.2D
92.73 AX-109261081
93.14 AX-109785183
94.47 AX-109879970 QSLt-2D
96.74 AX-111066402 QSAt-2D
97.89 AX-110289516
103.81 AX-110035074
106.98 AX-108778157
108.45 AX-108735612
109.16 AX-108780711
110.40 AX-111198680
111.80 AX-94735076
117.33 AX-111914966
118.22 AX-109922575
120.68 AX-108730160
125.65 AX-108755872
127.31 AX-109285491
128.07 AX-108832290
QSWt-2D
132.53 AX-110274295
135.08 AX-110638095
136.68 Xwmc18
Chr.3A-1
90.14 AX-95207768
92.14 AX-95679334
92.44 AX-95653062
QSAm-3A
99.61 AX-95235020
104.09 AX-95658735
104.72 AX-109830585 QSWb-3A
106.89 AX-95659792 QSRAt-3A
108.21 AX-111167455 QSRAm-3A
111.94 AX-108871682
115.77 AX-94926348
117.04 AX-108843516
118.07 AX-110994431
118.72 AX-111710665
123.77 AX-110161651
125.48 AX-111635376 QSDb-3A
127.24 AX-110400859 QSRAb-3A
127.99 AX-94928188
132.16 AX-110376668
Chr.3A-2
66.33 AX-89583101
67.84 AX-110954719
70.81 AX-95148936
QSLt-3A
73.23 AX-95658831
75.03 AX-94483013
Chr.3D
0.00 AX-111005008
13.42 AX-108924575
15.75 AX-94381228
16.41 AX-111161196 QSAm-3D
27.02 AX-111521335
27.34 AX-110463721
28.96 AX-109270894
29.63 AX-110979305
30.50 AX-111479324
31.73 AX-108746323
36.29 AX-110011202
37.65 AX-111502511
39.99 AX-109303667
44.91 AX-94550177
49.84 AX-111713694
55.53 AX-111415109
57.70 AX-111440673
61.35 Xgdm72
62.41 AX-109101506
63.67 AX-108800061
64.30 AX-111969732
67.42 AX-108814800
68.03 AX-108977327
69.44 AX-110558400
70.82 AX-110394178
72.71 Xgwm341
74.02 AX-108859112
75.39 AX-108735265
77.13 AX-108745742 QSWm-3D
79.46 AX-108726498 QSWb-3D
81.46 Xgdm8
Chr.4B
112.38 AX-95007745
113.91 AX-94979447
114.68 AX-109464953
QSWt-4B
116.37 Xwmc47
126.32 AX-94711253
127.28 AX-94958222
Chr.5A-1
0.00 AX-95684142
0.89 AX-94513819
11.24 AX-110540989
12.56 AX-111662464
QSDt-5A
QSDm-5A
QSRAt-5A
19.48 AX-95683796
20.27 AX-111698638
22.77 AX-94871207
Chr.5A-2
6.44 AX-111632587
7.96 AX-95202017
8.73 AX-110976396 QSAt-5A
12.71 AX-95658960
18.79 AX-95684066
19.59 AX-95659236 QSWb-5A
22.72 AX-109921026
26.75 AX-95659825 QSAb-5A-1
30.22 AX-111799065
34.18 AX-94818117
34.65 AX-111219220
35.42 AX-111679689
36.01 AX-109035033
38.96 AX-111059577
40.67 AX-94729189
41.81 AX-110034913
42.57 AX-111474443
43.73 AX-112286299
49.23 AX-108938187 QSLb-5A
54.38 AX-95152679 QSLt-5A
56.72 AX-94406985 QSLm-5A
58.02 AX-110074871
62.50 AX-111580018
65.02 AX-111789373
68.12 Xwmc340 QSAb-5A-2
Chr.5A-3
49.39 AX-95652927
50.24 AX-94958942
50.84 AX-94402053
52.95 AX-95630862
53.66 AX-95630256
QSDb-5A
57.00 Xgwm291

Figure 4

Distribution of QTLs for stoma-related traits on a high-density linkage map.

To better display the QTLs, the high-density linkage maps show only markers near the QTL intervals. The QTLs with red fonts indicates that they were detected in both years

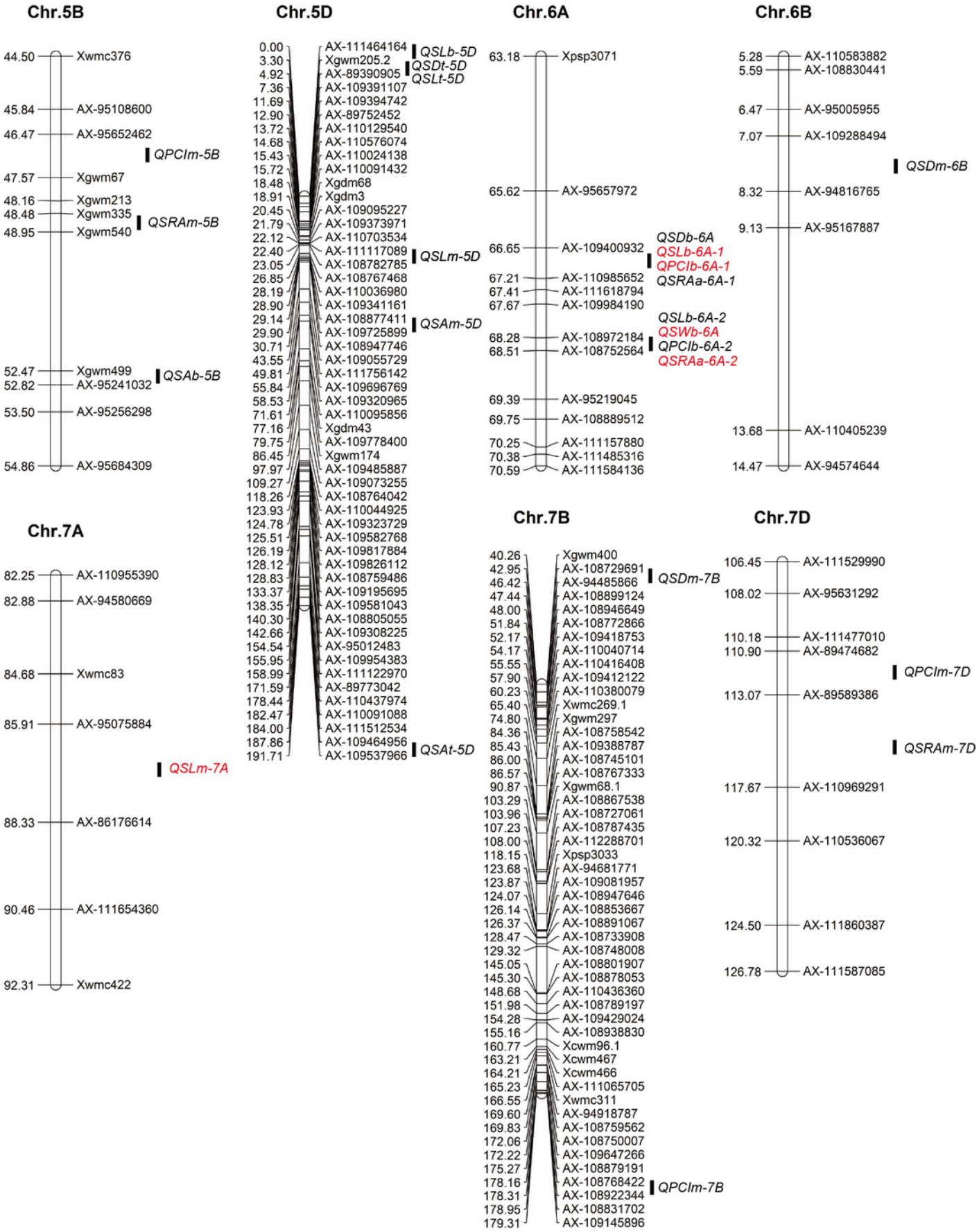
Chr.5B
44.50 Xwmc376
45.84 AX-95108600
46.47 AX-95652462
QPCIm-5B
47.57 Xgwm67
48.16 Xgwm213
48.48 Xgwm335
QSRAm-5B
48.95 Xgwm540
52.47 Xgwm499
QSAb-5B
52.82 AX-95241032
53.50 AX-95256298
54.86 AX-95684309
Chr.5D
0.00 AX-111464164
QSLb-5D
3.30 Xgwm205.2
QSDt-5D
4.92 AX-89390905
QSLt-5D
7.36 AX-109391107
11.69 AX-109394742
12.90 AX-89752452
13.72 AX-110129540
14.68 AX-110576074
15.43 AX-110024138
15.72 AX-110091432
18.48 Xgdm68
18.91 Xgdm3
20.45 AX-109095227
21.79 AX-109373971
22.12 AX-110703534
22.40 AX-111117089
QSLm-5D
23.05 AX-108782785
26.85 AX-108767468
28.19 AX-110036980
28.90 AX-109341161
29.14 AX-108877411
QSAm-5D
29.90 AX-109725899
30.71 AX-108947746
43.55 AX-109055729
49.81 AX-111756142
55.84 AX-109696769
58.53 AX-109320965
71.61 AX-110095856
77.16 Xgdm43
79.75 AX-109778400
86.45 Xgwm174
97.97 AX-109485887
109.27 AX-109073255
118.26 AX-108764042
123.93 AX-110044925
124.78 AX-109323729
125.51 AX-109582768
126.19 AX-109817884
128.12 AX-109826112
128.83 AX-108759486
133.37 AX-109195695
138.35 AX-109581043
140.30 AX-108805055
142.66 AX-109308225
154.54 AX-95012483
155.95 AX-109954383
158.99 AX-111122970
171.59 AX-89773042
178.44 AX-110437974
182.47 AX-110091088
184.00 AX-111512534
187.86 AX-109464956
QSAt-5D
191.71 AX-109537966
Chr.6A
63.18 Xpsp3071
65.62 AX-95657972
66.65 AX-109400932
QSDb-6A
QSLb-6A-1
QPCIb-6A-1
QSRAa-6A-1
67.21 AX-110985652
67.41 AX-111618794
67.67 AX-109984190
QSLb-6A-2
QSWb-6A
68.28 AX-108972184
QPCIb-6A-2
68.51 AX-108752564
QSRAa-6A-2
69.39 AX-95219045
69.75 AX-108889512
70.25 AX-111157880
70.38 AX-111485316
70.59 AX-111584136
Chr.6B
5.28 AX-110583882
5.59 AX-108830441
6.47 AX-95005955
7.07 AX-109288494
QSDm-6B
8.32 AX-94816765
9.13 AX-95167887
13.68 AX-110405239
14.47 AX-94574644
Chr.7A
82.25 AX-110955390
82.88 AX-94580669
84.68 Xwmc83
85.91 AX-95075884
QSLm-7A
88.33 AX-86176614
90.46 AX-111654360
92.31 Xwmc422
Chr.7B
40.26 Xgwm400
42.95 AX-108729691
QSDm-7B
46.42 AX-94485866
47.44 AX-108899124
48.00 AX-108946649
51.84 AX-108772866
52.17 AX-109418753
54.17 AX-110040714
55.55 AX-110416408
57.90 AX-109412122
60.23 AX-110380079
65.40 Xwmc269.1
74.80 Xgwm297
84.36 AX-108758542
85.43 AX-109388787
86.00 AX-108745101
86.57 AX-108767333
90.87 Xgwm68.1
103.29 AX-108867538
103.96 AX-108727061
107.23 AX-108787435
108.00 AX-112288701
118.15 Xpsp3033
123.68 AX-94681771
123.87 AX-109081957
124.07 AX-108947646
126.14 AX-108853667
126.37 AX-108891067
128.47 AX-108733908
129.32 AX-108748008
145.05 AX-108801907
145.30 AX-108878053
148.68 AX-110436360
151.98 AX-108789197
154.28 AX-109429024
155.16 AX-108938830
160.77 Xcwm96.1
163.21 Xcwm467
164.21 Xcwm466
165.23 AX-111065705
166.55 Xwmc311
169.60 AX-94918787
169.83 AX-108759562
172.06 AX-108750007
172.22 AX-109647266
175.27 AX-108879191
178.16 AX-108768422
QPCIm-7B
178.31 AX-108922344
178.95 AX-108831702
179.31 AX-109145896
Chr.7D
106.45 AX-111529990
108.02 AX-95631292
110.18 AX-111477010
110.90 AX-89474682
QPCIm-7D
113.07 AX-89589386
QSRAm-7D
117.67 AX-110969291
120.32 AX-110536067
124.50 AX-111860387
126.78 AX-111587085

Figure 5

The locations of two QTL hotspots on chromosome and the candidate genes contained in the two regions.

(a) LOD value of each traits. The line indicates the position where LOD is equal to 2.5. SD, stomatal density; SL, stomatal length; SW, stomatal width; PCI, potential conductance index; SRA, stomatal relative area; b, base of glumes. (b) Heat maps of expression of candidate genes contained in the two regions in wheat spikelets and glumes. The five genes below the red arrow are candidate genes that were screened out in this study

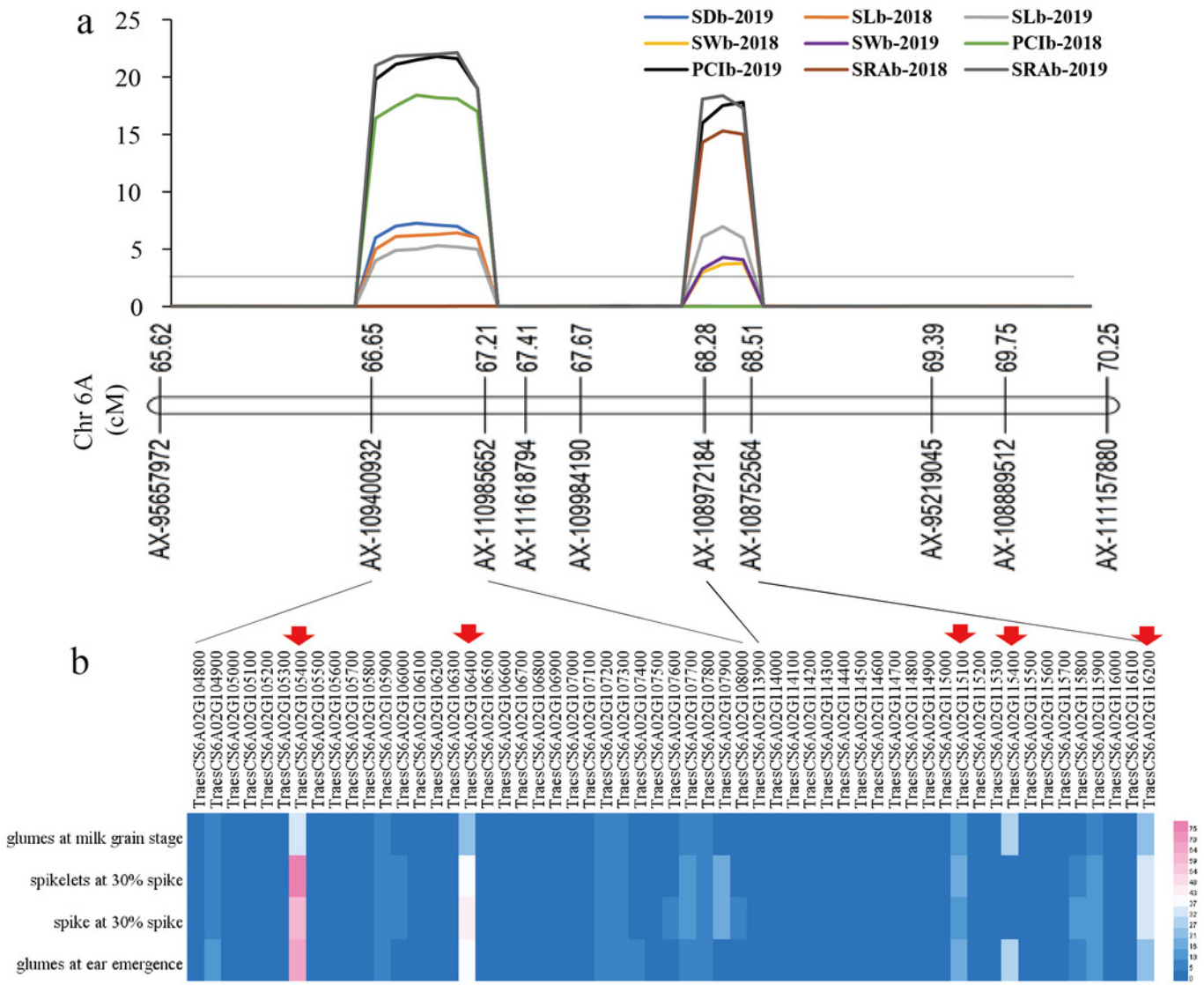
a
SDb-2019
SLb-2018
SLb-2019
SWb-2018
SWb-2019
PCIb-2018
PCIb-2019
SRAb-2018
SRAb-2019
25
20
15
10
5
0
Chr 6A (cM)
65.62
66.65
67.21
67.41
67.67
68.28
68.51
69.39
69.75
70.25
AX-95657972
AX-109400932
AX-110985652
AX-111618794
AX-109984190
AX-108972184
AX-108752564
AX-95219045
AX-108889512
AX-111157880
b
glumes at milk grain stage
spikelets at 30% spike
spike at 30% spike
glumes at ear emergence

Figure 6

Expression of candidate genes under various abiotic stresses.

(a) low phosphorus stress; (b) drought and heat stress; (c) salt stress

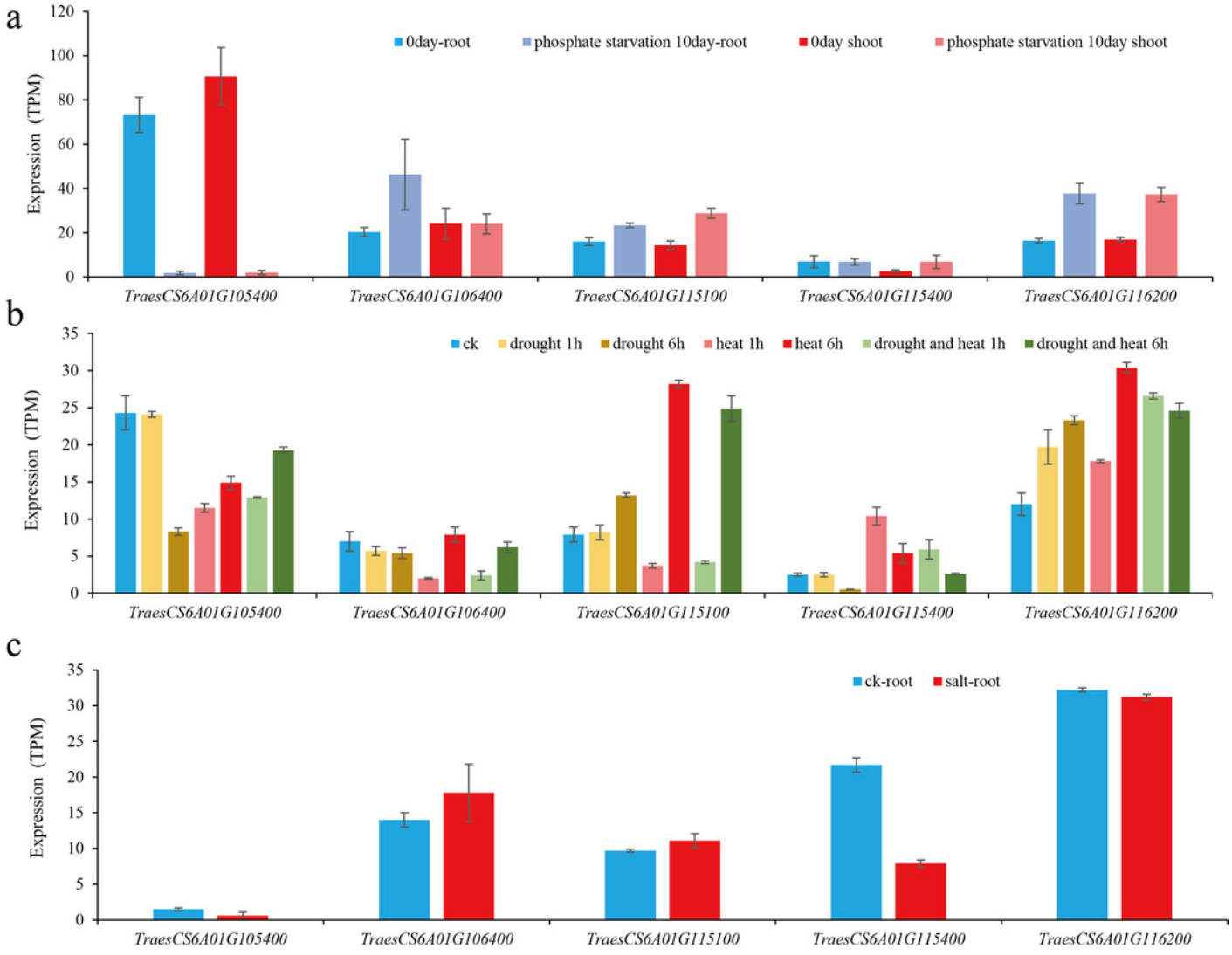

Table 1(on next page)

Phenotypic variation of stoma-related traits of wheat glumes in the DH population and parents.

[a] SD, stomatal density; SL, stomatal length; SW, stomatal width; PCI, potential conductance index; SA, stomatal area; SRA, stomatal relative area ; t, top of glumes; m, middle of glumes; b, base of glumes .

[b] Different letters after the values in a column indicate significant differences between two years.

[c] * and ** indicate significance at p-value <0.05 and p-value <0.01, respectively.

Table 1 Phenotypic variation of stoma-related traits of wheat glumes in the DH population and parents.

Traits[a]	Environments	Parents		Difference[c]	DHlines						
		Hanxuan10[b]	Lumai14[b]		Min	Max	Mean[b]	SD	Skewness	Kurtosis	CV (%)
SDt (No./mm^2)	2018	89.79a/A	81.63a/A	8.16*	60.21	111.44	85.43a/A	10.50	-0.37	0.81	12.29%
	2019	88.15a/A	74.12b/B	14.03**	59.41	106.87	78.99b/B	8.95	-0.91	3.67	11.33%
SDm (No./mm^2)	2018	80.27a/A	77.16a/A	3.15	52.03	112.20	78.33a/A	10.42	0.28	0.26	13.30%
	2019	82.17a/A	61.49b/B	20.68**	50.24	94.47	73.56b/B	9.14	-0.85	2.11	12.42%
SDb (No./mm^2)	2018	75.35b/A	74.01a/A	1.34	43.54	105.46	72.38a/A	10.92	0.16	0.34	15.08%
	2019	82.05a/A	63.13b/A	18.92**	40.01	103.90	69.17a/A	11.08	-0.31	1.98	16.02%
SLt (μm)	2018	45.60a/A	47.58a/A	-1.98	39.76	50.83	45.71a/A	2.42	-0.17	-0.61	5.29%
	2019	45.08a/A	45.19a/A	-0.11	40.03	50.25	45.67a/A	2.07	-0.16	-0.51	4.53%
SLm (μm)	2018	48.42a/A	46.85a/A	1.57	39.19	51.76	45.99a/A	2.32	-0.09	-0.23	5.04%
	2019	44.50b/A	46.75a/A	-2.25*	40.11	50.97	46.11a/A	2.24	-0.35	-0.13	4.86%
SLb (μm)	2018	48.73a/A	46.96a/A	1.77	38.33	51.25	45.22a/A	2.59	-0.11	-0.19	5.73%
	2019	45.15a/A	47.06a/A	-1.91*	38.63	50.50	44.70a/A	2.40	-0.03	-0.50	5.37%
SWt (μm)	2018	27.47a/A	34.55a/A	-7.08**	24.65	36.50	29.21a/A	2.42	1.06	2.23	8.28%
	2019	30.18a/A	28.93b/A	1.25	25.10	33.54	27.65b/B	1.29	1.28	3.08	4.67%
SWm (μm)	2018	30.45a/A	30.80a/A	-0.35	25.53	35.54	29.57a/A	2.22	0.86	1.02	7.51%
	2019	29.03a/A	29.55a/A	0.52	24.72	33.00	27.86b/B	1.58	0.53	0.64	5.67%
SWb (μm)	2018	30.80a/A	31.53a/A	-0.73	24.83	35.91	29.34a/A	2.48	0.79	1.08	8.45%
	2019	29.45a/A	32.36a/A	-2.91*	23.82	34.38	27.59b/B	1.88	0.95	1.40	6.81%
PCIt	2018	19.67a/A	17.91a/A	1.76	9.95	23.49	17.79 a/A	2.20	-0.04	1..01	12.37%
	2019	17.74a/A	14.88a/A	2.86	5.78	22.31	16.45 a/A	1.89	-0.77	2.78	11.49%
PCIm	2018	17.82a/A	16.77a/A	1.05	9.55	22.93	16.51 a/A	2.01	0.18	1.20	12.17%
	2019	16.31a/A	13.22b/B	3.09*	5.51	19.93	15.60 a/A	1.96	-0.76	1.97	12.56%
PCIb	2018	17.79a/A	16.40a/A	1.39	7.63	21.51	14.75 a/A	2.24	0.09	0.62	15.18%
	2019	16.53a/A	13.75a/A	2.78**	4.86	23.28	13.79 a/A	2.30	-0.04	1.58	16.68%
SAt (μm^2)	2018	1123.29a/A	1032.60a/A	90.69*	849.26	1397.99	1050.23 a/A	109.82	0.65	0.65	10.46%

	2019	1021.78a/A	986.60a/A	35.18	830.49	1258.00	991.41 a/A	65.37	0.48	1.21	6.59%
SAm (μm^2)	2018	944.15a/A	979.19a/A	-35.04	861.54	1460.76	1069.71 a/A	102.88	0.50	0.85	9.62%
	2019	996.95a/A	1043.27a/A	-46.32**	818.67	1306.33	1009.14 a/A	83.93	0.44	0.84	9.47%
SAb (μm^2)	2018	1135.79a/A	1120.20a/A	15.59	799.39	1412.54	1044.39 a/A	119.29	0.61	0.36	8.32%
	2019	975.76a/A	1153.63a/A	-177.87**	784.21	1203.87	968.12 b/B	85.79	0.31	-0.40	8.86%
SRAt （%）	2018	9.96a/A	8.31a/A	1.65	4.56	12.16	8.94 a/A	1.20	0.01	0.74	13.42%
	2019	8.89a/A	7.23b/B	1.66	2.77	9.72	7.81 b/B	0.86	-0.96	2.74	11.01%
SRAm （%）	2018	9.09a/A	6.82a/A	2.27*	4.59	12.16	8.36 a/A	1.25	0.44	0.85	14.95%
	2019	8.08a/A	6.30b/A	1.78	2.62	10.24	7.40 a/A	0.97	-0.58	1.75	13.11%
SRAb （%）	2018	8.65a/A	8.52a/A	0.13	4.35	12.16	7.54 a/A	1.31	0.48	0.85	17.37%
	2019	7.96a/A	7.17a/A	0.79	2.34	11.79	6.68 b/A	1.17	0.25	1.91	17.51%

[a] SD, stomatal density; SL, stomatal length; SW, stomatal width; PCI, potential conductance index; SA, stomatal area; SRA, stomatal relative area; t, top of glumes; m, middle of glumes; b, base of glumes.

[b] Different letters after the values in a column indicate significant differences between two years.

[c] * and ** indicate significance at p-value <0.05 and p-value <0.01, respectively.

Table 2(on next page)

Quantitative trait loci (QTLs) for stoma-related traits of wheat glumes in DH population[a]

[a] LOD, LOD value of each QTL; PVE, phenotypic variance explained by QTL; Add, a positive sign means increased effect contributed by Hanxuan 10; a negative sign indicates increased effect contributed by Lumai 14.

[b] SD, stomatal density; SL, stomatal length; SW, stomatal width; PCI, potential conductance index; SA, stomatal area; SRA, stomatal relative area.

[c] Top, top of glumes; Middle, middle of glumes; Base, base of glumes. [d] Underlined QTLs indicate that they were detected in two years.

Table 2 Quantitative trait loci (QTLs) for stoma-related traits of wheat glumes in DH population[a]

Trait[b]	Location[c]	QTL[d]	Chr	Left marker	Right marker	2018			2019		
						LOD	PVE (%)	Add	LOD	PVE (%)	Add
SD	Top	*QSDt-2A*	2A	AX-95631506	AX-94664024	3.57	9.60	2.73	2.63	6.92	2.28
		QSDt-5A	5A	AX-111662464	AX-95683796	2.66	8.10	-2.94			
		QSDt-5D	5D	Xgwm205.2	AX-89390905				2.57	6.78	-2.25
	Middle	*QSDm-1A*	1A	AX-111105973	AX-94402739				2.82	8.89	2.66
		QSDm-5A	5A	AX-111662464	AX-95683796	3.77	8.74	3.37			
		QSDm-6B	6B	AX-109288494	AX-94816765				2.56	7.87	-2.47
		QSDm-7B	7B	AX-108729691	AX-94485866	3.02	6.92	-2.97			
	Base	*QSDb-3A*	3A	AX-111635376	AX-110400859	3.44	8.66	-3.37			
		QSDb-5A	5A	AX-95630256	Xgwm291				3.84	11.41	3.76
		QSDb-6A	6A	AX-109400932	AX-110985652				7.27	8.98	3.22
SL	Top	*QSLt-1A*	1A	AX-111105973	AX-94402739	5.60	11.33	-0.90			
		QSLt-1D	1D	AX-109929813	AX-94979481	3.70	7.31	-0.70			
		QSLt-2D	2D	AX-109879970	AX-111066402	5.22	11.06	0.76	4.49	9.26	-0.69
		QSLt-3A	3A	AX-95148936	AX-95658831	4.50	8.93	0.79			
		QSLt-5A	5A	AX-95152679	AX-94406985	3.36	6.55	-0.66			
		QSLt-5D	5D	Xgwm205.2	AX-89390905				2.54	5.45	0.53
	Middle	*QSLm-5A*	5A	AX-95152679	AX-94406985	2.79	5.07	-0.62			
		QSLm-5D	5D	AX-111117089	AX-108782785				2.88	8.68	0.65
		QSLm-7A	7A	AX-95075884	AX-86176614	5.61	10.57	0.96	3.31	6.05	-0.70
	Base	*QSLb-5A*	5A	AX-108938187	AX-95152679	3.26	9.53	-0.81			
		QSLb-5D	5D	AX-111464164	Xgwm205.2				2.94	9.18	0.70
		QSLb-6A-1	6A	AX-109400932	AX-110985652	6.42	9.64	1.17	5.31	8.97	1.01
		QSLb-6A-2	6A	AX-108972184	AX-108752564				6.97	9.59	-1.19
SW	Top	*QSWt-1D*	1D	AX-95141814	AX-95661009	2.83	7.89	-0.69			
		QSWt-2D	2D	AX-108832290	AX-110274295				3.86	11.31	-0.43
		QSWt-4B	4B	AX-109464953	Xwmc47	2.58	7.40	-0.67			
	Middle	*QSWm-3D*	3D	AX-108735265	AX-108745742				2.99	8.91	-0.47
	Base	*QSWb-3A*	3A	AX-95659792	AX-111167455				2.84	6.94	-0.52
		QSWb-3D	3D	AX-108735265	AX-108745742	2.63	10.59	-0.69			

		QSWb-5A	5A	AX-95659236	AX-109921026				3.32	8.19	-0.57
		QSWb-6A	6A	AX-108972184	AX-108752564	3.47	8.74	-0.77	4.29	9.75	-0.77
PCI	Middle	*QPCIm-1D*	1D	AX-110935476	AX-95630666				2.65	3.63	-0.44
		QPCIm-2B	2B	AX-109283083	AX-95101397				4.15	5.82	0.57
		QPCIm-5B	5B	AX-95652462	Xgwm67				11.52	19.02	-1.03
		QPCIm-7B	7B	AX-108768422	AX-108922344				3.72	5.19	-0.53
		QPCIm-7D	7D	AX-89474682	AX-89589386				5.26	7.52	-0.64
	Base	*QPCIb-1D*	1D	AX-95141814	AX-95661009				2.71	4.56	-0.59
		QPCIb-6A-1	6A	AX-109400932	AX-110985652	18.42	13.64	3.55	21.79	14.06	3.15
		QPCIb-6A-2	6A	AX-108972184	AX-108752564				17.81	8.65	-2.47
SA	Top	*QSAt-1D*	1D	AX-94979481	AX-109507293	3.86	6.87	-42.97			
		QSAt-2A	2A	Xcwm138.2	AX-110686688	4.12	9.25	-50.09			
		QSAt-5A	5A	AX-95202017	AX-110976396	5.14	9.28	-50.40			
		QSAt-2D	2D	AX-109879970	AX-111066402	5.24	8.73	31.24	8.40	13.96	-38.91
		QSAt-5D	5D	AX-109464956	AX-109537966				2.92	4.45	-22.28
	Middle	*QSAm-1D*	1D	AX-94979481	AX-109507293	4.36	10.99	-43.05			
		QSAm-3A	3A	AX-95653062	AX-95235020	3.68	9.18	-39.55	3.01	7.42	-35.62
		QSAm-3D	3D	AX-94381228	AX-111161196				3.16	9.18	-31.81
		QSAm-5D	5D	AX-108877411	AX-109725899				2.71	7.88	28.75
	Base	*QSAb-5A-1*	5A	AX-95659825	AX-111799065				7.45	13.27	-46.15
		QSAb-2A	2A	Xcwm138.2	AX-110686688				6.14	12.89	-44.81
		QSAb-5A-2	5A	AX-111789373	Xwmc340	2.61	7.88	-42.04			
		QSAb-5B	5B	Xgwm499	AX-95241032				3.81	6.65	-32.36
SRA	Top	*QSRAt-3A*	3A	AX-95659792	AX-111167455	3.20	8.56	-0.35			
		QSRAt-5A	5A	AX-111662464	AX-95683796	3.94	11.30	-0.40			
	Middle	*QSRAm-3A*	3A	AX-95659792	AX-111167455	2.66	10.30	-0.35			
		QSRAm-5B	5B	Xgwm335	Xgwm540				5.15	12.63	-0.36
		QSRAm-7D	7D	AX-89589386	AX-110969291				3.97	9.51	-0.31
	Base	*QSRAb-1A*	1A	AX-111764211	AX-111262687	2.51	7.15	-0.35			
		QSRAb-3A	3A	AX-111635376	AX-110400859	4.58	13.48	-0.46			
		QSRAb-6A-1	6A	AX-109400932	AX-110985652				22.12	10.74	1.68
		QSRAb-6A-2	6A	AX-108972184	AX-108752564	15.31	8.89	-1.39	18.38	6.82	-1.34

[a] LOD, LOD value of each QTL; PVE, phenotypic variance explained by QTL; Add, a positive sign means increased effect contributed by Hanxuan 10; a negative sign indicates increased effect contributed by Lumai 14.

[b] SD, stomatal density; SL, stomatal length; SW, stomatal width; PCI, potential conductance index; SA, stomatal area; SRA, stomatal relative area.

[c] Top, top of glumes; Middle, middle of glumes; Base, base of glumes.

[d] Underlined QTLs indicate that they were detected in two years.

Table 3(on next page)

Candidate genes screened from QTL regions in this study

1 Table 3 Candidate genes screened from QTL regions in this study

2

Gene ID	Gene annotation
TraesCS6A02G105400	50S ribosomal protein L3
TraesCS6A02G106400	Stress-associated endoplasmic reticulum protein 2
TraesCS6A02G115100	Purple acid phosphatase
TraesCS6A02G115400	Calcium-dependent lipid-binding (CaLB domain) family
TraesCS6A02G116200	ATP-dependent RNA helicase

3